

^4He Crystal Quality and Rotational Response in a Transparent Torsional Oscillator

A. D. Fefferman, X. Rojas, A. Haziot, and S. Balibar

*Laboratoire de Physique Statistique de l'Ecole Normale Supérieure,
associé au CNRS et aux Universités Denis Diderot et P.M Curie,
24 rue Lhomond 75231 Paris Cedex 05, France*

J. T. West and M. H. W. Chan

*Department of Physics, The Pennsylvania State University,
University Park, Pennsylvania 16802, USA*

(Received textdate)

Abstract

We have studied natural purity ^4He single crystals and polycrystals between 10 and 600 mK using a torsional oscillator with a 2 cm^3 rigid cell made of sapphire with a smooth geometry. As the temperature was lowered, we observed sample dependent but reproducible resonant frequency shifts that could be attributed to a supersolid fraction of order 0.1%. However, these shifts were observed with single crystals, not with polycrystals. Our results indicate that, in our case, the rotational anomaly of solid helium is more likely due to a change in stiffness than to supersolidity. This interpretation would presumably require gliding of dislocations in more directions than previously thought.

PACS numbers: 67.80.bd, 67.80.B-, 61.72.Lk

I. INTRODUCTION

In 2004, Kim and Chan^{1,2} discovered a rotational anomaly in torsional oscillator (TO) measurements on solid ^4He and proposed that it was due to supersolidity. In measurements of the shear modulus of solid ^4He , Day and Beamish³ observed a softening of the solid with the same dependence on temperature and ^3He concentration as that of the resonant frequency shift in TO measurements. The softening was attributed to the evaporation of ^3He impurities from dislocations as the temperature T increased above 100 to 200 mK. It was a surprise to realize that, in its “supersolid” state where part of the mass is supposed to flow through the rest of the solid, this solid was actually stiffer than when no flow is observed.⁴ However, this apparent contradiction was tentatively explained by assuming that mass superflow occurs in the core of dislocations only if the latter are not free to move.⁴ According to this scenario, the rotational anomaly (i.e. the supersolidity) and the elastic anomaly (the change in stiffness) could be two consequences of a single phenomenon, namely the binding/unbinding of ^3He impurities to dislocations.

At the same time, one realized that, as T was lowered, both an inertia decrease due to the appearance of supersolidity and a stiffening due to dislocation pinning should induce an increase of the TO resonance frequency.^{5,6} Moreover, J.D. Reppy observed a large frequency shift that was not consistent with supersolidity and more likely due to a stiffness change.⁷ When a TO is made of several parts that are not rigidly bound together, as is the case in Reppy’s experiment, the TO frequency shift may reach several percent of the “mass loading” - the shift due to filling the TO with solid ^4He . We understand this as a “glue effect”, which means that solid ^4He glues parts together so that any change in the stiffness of solid ^4He has a large effect on the TO frequency. On the other hand, very rigid TOs with a simpler geometry should not exhibit this glue effect and the magnitude of the elastic effect has been much smaller. This is the case with the TO used by West et al.⁸ where the frequency shift was about 0.015% and the calculated contribution from the stiffness change 60 times smaller.

As a consequence one should check in every experiment whether a rotational anomaly in a TO measurement originates from a change in the inertia or in the elastic coefficient (Ref. 9). For this reason we have built a simple and rigid TO with a sapphire “minibottle” that could be filled either with a single crystal or with a polycrystal (Fig. 1). If one assumes that superflow in a supersolid takes place inside defects, the magnitude of the superfluid fraction

should increase with disorder and it should be *smaller* in single crystals than in polycrystals. This would be consistent with measurements by Clark et al.¹⁰ As for elastic properties, Rojas *et al.*¹¹ showed that single crystals have a *larger* stiffness anomaly than polycrystals.³ The softening observed in the crystals is consistent with a 50 to 86% decrease in the elastic coefficient c_{44} whereas that in the polycrystals is due to a 7 to 15% decrease in the effective shear modulus μ . Based on these numbers, one would expect a larger frequency shift for a single crystal than for a polycrystal if the rotation anomaly is controlled by elasticity.⁵ Our comparison of single crystals to polycrystals in a sapphire TO could thus discriminate between the two possible origins of rotational anomalies. As we shall see below, we observed a larger effect with single crystals, a result that is not consistent with the supersolid scenario.

We first verified that growth at constant volume from the normal liquid using the “blocked capillary method” produces polycrystals whose grain boundaries could be seen during melting, while growth from the superfluid on the melting line produces single crystals without grain boundaries and with easily visible facets.^{12–14} As we shall see below, we found that in our TO the rotation anomaly for a polycrystal is below the resolution of our measurement, if it exists. On the opposite, we found definite frequency shifts for single crystals. The magnitudes of these frequency shifts were reproducible when measured with the same crystal, but they varied from one single crystal to another, as expected from recent calculations, if the crystal orientation with respect to the rotation axis changed.⁵

II. EXPERIMENT

Our transparent sapphire minibottle sits atop a coin silver torsion rod (Fig. 1). The sample volume in our cell has a cylindrical geometry with a hemispherical part at the top to which the fill line was glued with Stycast 1266. This cell shape has no sharp corners. It was chosen to obtain a rigid cell that could be filled by solid helium without leaving liquid regions behind during crystallization when the liquid-solid interface goes up from the bottom. It also minimized the risk of facet blocking as the single crystals reached the neck at the top of the minibottle. The cylindrical section had an inner diameter of 11.1 mm and a height of 15.2 mm. The growth of polycrystals at constant volume started at 2.55 K and finished at 1.97 K, implying that the final pressure in the solid was 38 bar. This TO resonates near 910 Hz. The “mass loading” was 1.8 Hz. All measurements shown here were done with the

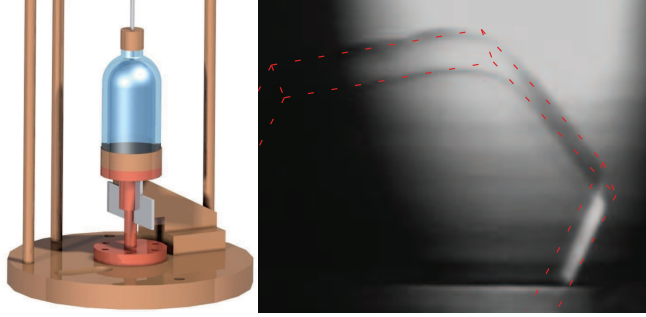


FIG. 1: (color) The TO (left) is filled from the top and is bolted to a vibration isolation stage that is suspended from the dilution refrigerator mixing chamber. For clarity, the second electrode structure (placed diagonally from the displayed electrode structure) and the fourth suspension rod are omitted from this drawing. Right panel: Photograph of an hcp single crystal grown at 20 mK and 25.3 bar that partially fills the TO cell. The image is dark at the edges due to refraction. The dashed red lines illustrate the hexagonal shape of the crystal.

fill line of the 1K stage closed in order to minimize mechanical vibrations.

We have grown many crystals in this cell. For clarity we present the last three ones for which the best stability and reproducibility was obtained after optimization of our methods. The sample labeled “single crystal #1” was first grown at 10 mK with a growth speed $\approx 10 \mu\text{m/s}$. Before any further treatment, the TO results in this crystal were not reproducible as a function of time. Random jumps of order 1 mHz always occurred during the temperature scan (12 hours). These jumps made it impossible to achieve the stable resolution we needed (0.1 mHz). Apparently, when a high quality crystal is in equilibrium with liquid ^4He at the orifice of the fill line, some mass spontaneously rearranges somewhere, which makes the TO frequency unstable. We had to escape from the liquid-solid equilibrium to obtain stable measurements. This was achieved by warming the crystal to 1.4 K, melting 10% of the crystal and then regrowing it with a growth speed $\approx 3 \mu\text{m/s}$. At 1.4 K, no facet could block the growth near the orifice of the fill line.¹³ Furthermore, if a small amount of liquid still remained in the cell at 1.4 K, it would have solidified very soon after cooling started.¹² Since cooling below 1.4 K along the melting line changes the cell pressure, some anisotropic stresses may have produced some dislocations in this single crystal until all the liquid space including the fill line had solidified. Single crystal #2 was obtained in the same way but grown from a different seed. This crystal was warmed up to 1.45 K, at which point 20%

of the crystal was melted and regrown. In single crystals grown at 1.4 K, Syshchenko and Beamish¹⁵ measured a dislocation density in the range 10^3 to 10^5 cm^{-2} . We estimate that this dislocation density is approximately equal to or possibly greater than the density in our single crystals.

We primarily operated the TO at constant response amplitude and constant drive frequency, extracting the resonant frequency, f_0 , and quality factor, Q , from the phase of the TO response and the drive level with a method similar to that of Ref. 16. This method is different from the more widely used phase locked loop where the response amplitude and the drive frequency are not kept constant while scanning the temperature. We used the circuit shown in Fig. 2 for our measurement. The long heavy black line in the dashed box represents the mobile electrodes of the TO and the short heavy black lines represent the fixed electrodes. The spacing between the electrodes, d , is 90 microns, yielding a capacitance $C = 3$ pF. A bias voltage $V = 260$ V is applied to the mobile electrodes via the current limiting resistor $R = 2$ M Ω . A function generator is used to apply an ac voltage, \tilde{V} , on the order of millivolts to the drive electrode. The motion in response to the resulting torque modulates the spacing and causes a current

$$I = \frac{-i\omega CVl\theta}{d} \quad (1)$$

to flow into the current amplifier, since the voltage across the detection capacitor remains constant. In Eq. 1, ω is the drive angular frequency, $l = 7.6$ mm is the radial position of the detection electrode, and $\theta = \theta_0 e^{i(\omega t + \alpha)}$ is the angular position of the mobile electrodes, where α is the phase angle relative to \tilde{V} . The lockin amplifier then measures a voltage

$$V_{LI} = IG e^{i\phi}, \quad (2)$$

where $G = 10^8$ V/A is the gain of the current amplifier and ϕ is the phase shift due to the measurement electronics.

The susceptibility $\chi(\omega)$ characterizes the response, θ , of a TO to an externally applied torque, τ . Our TO is well described by the form

$$\chi^{-1} = \tau/\theta = J\omega^2 - ib\omega - k, \quad (3)$$

where the coefficients J, b and k may be temperature dependent. We have defined χ so that a positive static torque decreases θ . The resonant frequency ω_0 and Q of the TO are related

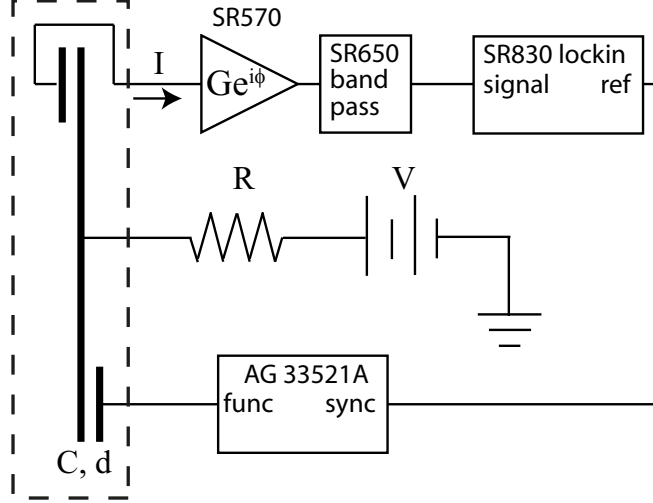


FIG. 2: The circuit used to measure the resonant frequency and Q of the torsional oscillator. The components in the dashed box are at the temperature of the mixing chamber. The lockin amplifier and function generator are controlled via a GPIB interface.

to the root of χ^{-1} (Ref. 17). We obtain

$$\omega_0 = \sqrt{\frac{k}{J}} \quad (4)$$

and

$$Q^{-1} = \frac{b}{\omega_0 J}. \quad (5)$$

One way we determined ω_0 and Q of the TO was by measuring the response of the TO at constant temperature and drive level while sweeping the drive frequency through the resonance (a “frequency sweep”). We fit the function

$$V_{LI} = \frac{-i\tilde{F}\omega}{(\omega_0^2 - \omega^2 + iQ^{-1}\omega\omega_0)} Ge^{i\phi} \quad (6)$$

to the TO response as measured by the lockin amplifier. Eq. 6 was derived from Eqs. 1, 2, and 3. The fitting parameters in Eq. 6 are the resonant frequency, ω_0 ; the quality factor of the TO, Q ; the phase shift introduced by the measurement electronics, ϕ ; and \tilde{F} , which is proportional to \tilde{V} . An example of a frequency sweep is given in Fig. 3. The best fit values of $\omega_0/2\pi$ and Q^{-1} from the frequency sweeps are plotted as large filled circles in Figs. 4-6. The color of the circle indicates that the frequency sweep (at constant temperature) was carried out soon before or after the temperature sweep with the same color.

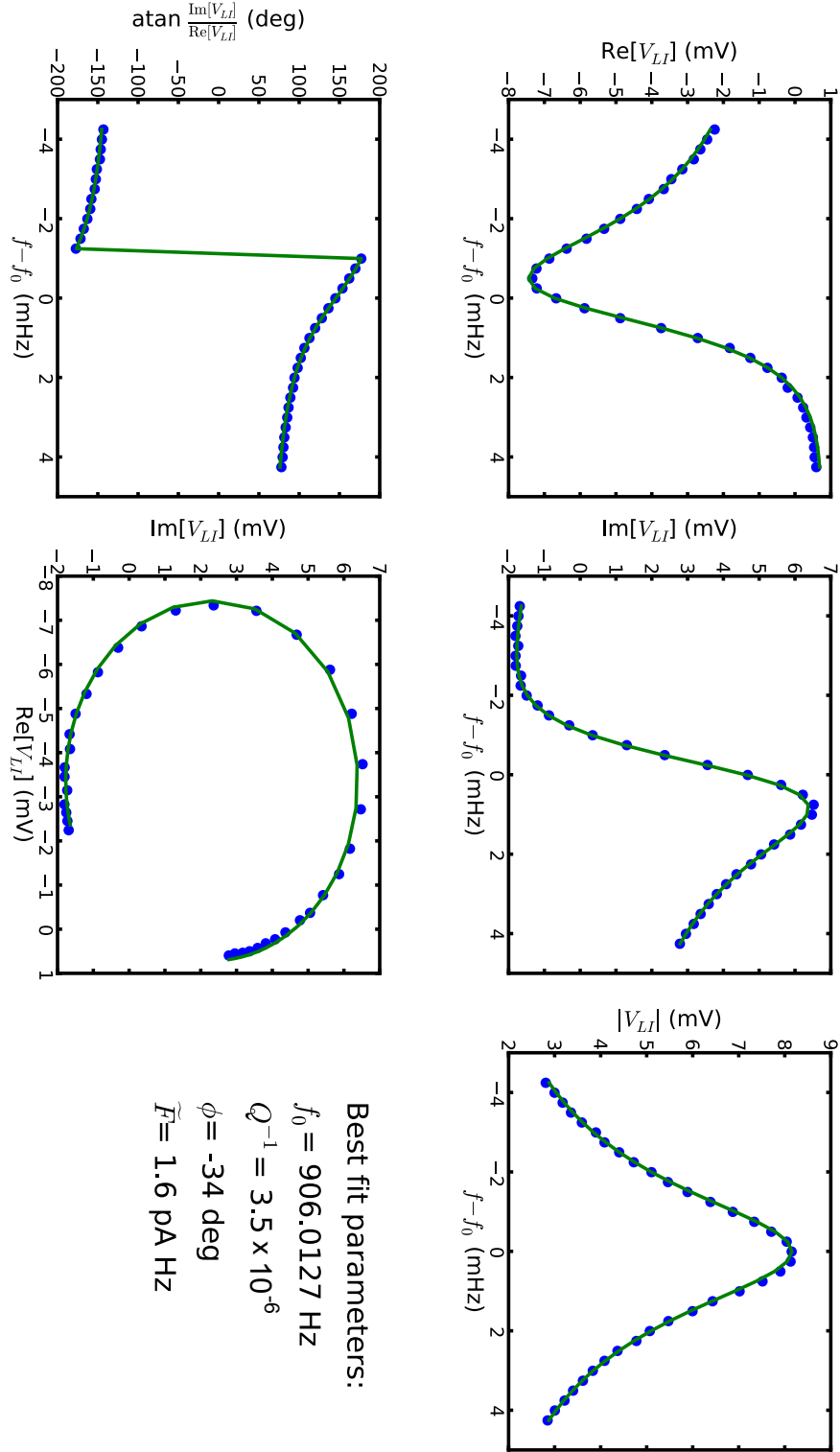


FIG. 3: (color online) Response of the torsional oscillator with the polycrystalline sample discussed in the text, measured using the circuit in Fig. 2.

The TO f_0 and Q were measured at constant drive frequency and constant response amplitude for the temperature sweeps. Substituting $\tau = \tau_0 e^{i(\omega t + \pi)}$ and $\theta = \theta_0 e^{i(\omega t + \alpha)}$ into Eq. 3, we obtain

$$\tau_0 e^{i(\pi - \alpha)} + k\theta_0 + ib\omega\theta_0 - J\omega^2\theta_0 = 0. \quad (7)$$

Taking the real part of Eq. 7, we obtain

$$\omega_0^2 = \omega^2 \left(1 + \frac{\tau_0 \cos \alpha}{J\omega^2\theta_0} \right). \quad (8)$$

We then make the approximation $k = J\omega^2$ in Eq. 8, since $(\omega - \omega_0)/2\pi < 20$ mHz for our measurements, yielding

$$\omega_0^2 = \omega^2 \left(1 + \frac{\dot{\tau}_0 \cos \alpha}{k\dot{\theta}_0} \right). \quad (9)$$

Furthermore, we note that $\tau_0/k = \theta_R/Q$, where $\theta_R \equiv \theta_0$ at the resonant frequency. Since the relative variation of ω_0 over the entire temperature range of our measurements is only $\approx 10^{-5}$, k is nearly independent of temperature. Thus, $\dot{\tau}_0/k |\tilde{V}| = \dot{\theta}_R/Q |\tilde{V}| = 3.9 \times 10^{-6} \text{ sec}^{-1}\text{V}^{-1} \equiv c$ is also nearly independent of temperature, and when this is substituted into Eq. 9, we obtain

$$\omega_0 = \omega \sqrt{1 + \frac{c |\tilde{V}| \cos \alpha}{\dot{\theta}_0}}. \quad (10)$$

Taking the imaginary part of Eq. 7, we obtain

$$Q^{-1} = -\frac{\tau_0 \sin \alpha}{J\omega_0\omega\theta_0}. \quad (11)$$

Using the same approximations that were used to obtain Eq. 10, we obtain

$$Q^{-1} = -\frac{c |\tilde{V}| \sin \alpha}{\dot{\theta}_0}. \quad (12)$$

Holding $\dot{\theta}_0$ constant, we determined ω_0 and Q^{-1} by measuring α and $|\tilde{V}|$.

Before doing a temperature sweep, we set the drive frequency to minimize $\omega - \omega_0$ over the temperature range of the measurement. The drive level was set so that the desired TO rim speed was approximately obtained at the starting temperature of the temperature sweep. At this point, we began to constantly acquire the value of V_{LI} from the lockin amplifier. The TO was allowed to equilibrate for 8 minutes at the initial drive level. The values of ω_0 and Q^{-1} were then determined by applying Eqs. 10 and 12 and averaging over the next 4 minutes. The drive level was then adjusted, if necessary, to obtain exactly the desired TO rim speed,

and the TO was allowed to equilibrate for 8 minutes again. The values of ω_0 and Q^{-1} at the desired rim speed were then obtained by averaging for 10 minutes. The temperature was then incremented or decremented, and the measurement routine was repeated.

III. RESULTS

In Fig. 4 we present example measurements of the resonant frequency shift δf of the TO *versus* temperature T for the three different samples. This shift is the difference between the actual TO frequency and a reference frequency. This reference frequency is adjusted for each sample so that the high temperature parts superimpose. The specified rim speeds are measured at the inner surface of the cylindrical portion of the minibottle. The frequency shift with the polycrystalline sample is linear in T above ≈ 80 mK, as found when the cell is filled with superfluid except for a different slope. Near 40 mK, the frequency shows a maximum which is known to be due to the TO fabrication materials as found by other groups.¹⁶ Thus, we see no evidence for a rotational anomaly within the resolution of our experiment (0.2 mHz). This means that, if it exists, the superfluid fraction is less than 10^{-4} in this polycrystal. It is also consistent with a change in μ of less than 15%,⁵ a reasonable value.³ This result is robust: for example, we show in Fig. 4 that the T dependence of the frequency shift is the same for rim speeds of 3 and 10 $\mu\text{m}/\text{sec}$ for both warming and cooling. But for the single crystal samples, δf departs from the linear T dependence in the intermediate temperature range.

The frequency shift for the two single crystal samples relative to the frequency shift for the polycrystal $\delta f - \delta f_{\text{pc}}$ is shown in Fig. 5. We compute the frequency shift relative to the polycrystal rather than a superfluid filled cell because the latter has a linear T dependence above 300 mK that is different from the solid ones, as found by other groups.¹⁸ The slope is 9 mHz/K when the cell and its fill line are filled with superfluid, compared with 8 mHz/K for the solid samples. Thus, computing $\delta f - \delta f_{\text{pc}}$ best exposes the relevant behavior. As the temperature was decreased, an increase in $\delta f - \delta f_{\text{pc}}$ was observed with a magnitude of 1 mHz (2 mHz) for single crystal #1 (#2). Our observation of a frequency shift with single crystals which is sample dependent but reproducible and definitely larger than with polycrystals is qualitatively consistent with shifts originating from a stiffness change, not an inertia change in our samples. In order to demonstrate reproducibility, several temperature

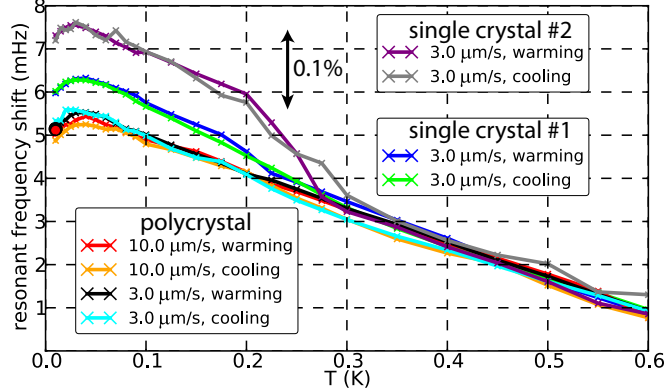


FIG. 4: (color) Temperature dependence of the resonant frequency shift δf for the polycrystal and two single crystals at the specified rim speeds. For the polycrystal, δf is linear above 80 mK, indicating the absence of a rotation anomaly to within the resolution of our measurement (0.2 mHz). The slightly amplitude dependent curvature below 80 mK is due to the T dependence of the TO fabrication materials. For single crystals #1 and #2, δf departs from the linear T dependence at intermediate temperatures. The red and black closed circles at 10 mK that verify our constant drive frequency measurements were obtained by fitting a Lorentzian to the TO resonant response. The scale bar relates the frequency shift to the TO mass loading (see text).

sweeps on both warming and cooling are shown for each crystal. There is no clear critical velocity over the range of rim speeds studied here: for single crystal #1, measurements at 0.5, 1.0 and 3.0 $\mu\text{m}/\text{sec}$ are the same within our resolution. A noticeable difference with other experiments is the temperature where the shift occurs. Half of it was completed at 200 mK for single crystal #1 and at 250 mK for single crystal #2. In contrast, other TO measurements or direct elastic measurements of natural purity (300 ppb) solid helium show that half of the frequency or stiffness shift is completed at 90 mK, as shown by the black dashed line in Fig. 5 from Beamish's results.³

The T dependence of the TO dissipation Q^{-1} is shown in Fig. 6. For the polycrystal, $Q^{-1}(T)$ has the standard T dependence generated by the TO fabrication materials: a temperature independent plateau above 200 mK with a roll-off below this temperature.¹⁶ There is no feature consistent with a rotational anomaly. For single crystal #2, the behavior is significantly different than that for the polycrystal, but reproducible. In Fig. 6, four T sweeps at 3 $\mu\text{m}/\text{sec}$ are shown for single crystal #2, two on warming and two on cooling. The damping is the same as that of the polycrystal below 150 mK, but exceeds that of the

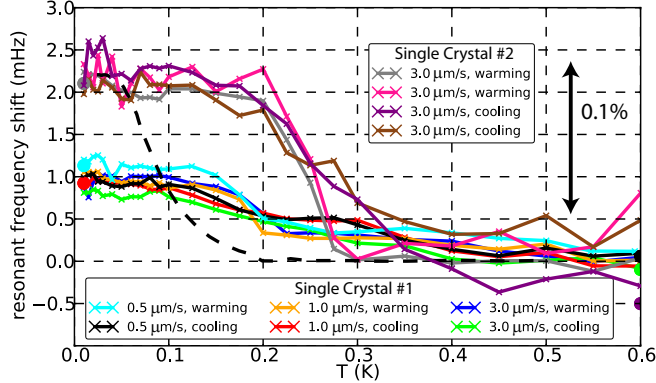


FIG. 5: (color) Temperature dependence of the TO resonant frequency shift δf for single crystals #1 and #2 relative to δf_{pc} for the polycrystal at the specified rim speeds. The T dependence observed in most other TO or elastic measurements on natural purity solid ^4He , represented by data from Ref. 3 (vertically scaled), is shown with a dashed black line for comparison. The six closed circles at 10 or 600 mK verify our measurements as explained in the Fig. 4 caption. The scale bar relates the frequency shift to the TO mass loading (see text).

polycrystal in part of the upper T range. There is a local maximum in the damping near 250 mK, coincident with the maximum rate of increase of δf , though the T dependence is qualitatively different for warming and cooling. The warming and cooling curves converge to the same damping level at 600 mK, closing the hysteresis loop. For single crystal #1, $Q^{-1}(T)$ reaches a small reproducible maximum at 200 mK on warming, which again coincides with the maximum rate of increase in the corresponding measurement of δf . The four closed circles are the best fit values of the dissipation for Lorentzians fitted to the resonant response of the TO, as discussed in reference to Figs. 4 and 5, validating the accuracy of our measurements at a constant drive frequency.

IV. DISCUSSION

Our observation of larger frequency shifts in single crystals than in polycrystals does not seem consistent with supersolidity since the density of dislocations along which the supersolid may flow is presumably at least as large in polycrystals as in single crystals. Thus softening of the crystals seems like the most likely explanation for our observations.^{3,21} One usually assumes that edge dislocations easily glide only parallel to the basal planes of

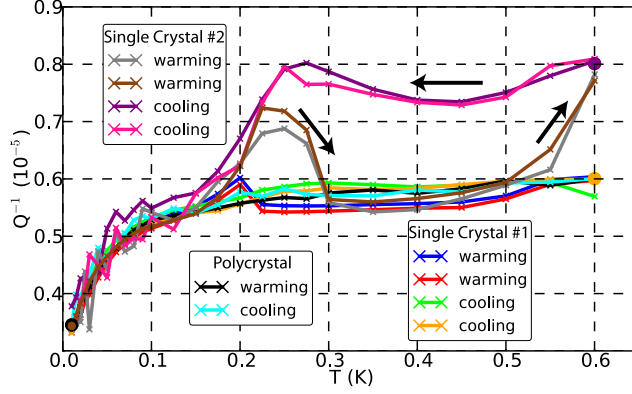


FIG. 6: (color) Temperature dependence of the TO dissipation for the polycrystal and both single crystals measured at a rim speed of $3 \mu\text{m}/\text{sec}$. The temperature of the prominent dissipation peak for single crystal #2 on warming coincides with the maximum of $|d(\delta f - \delta f_{\text{pc}})/dT|$ (Fig. 5). An offset of 8×10^{-7} , probably due to a temporary increase in the TO background damping, was subtracted from one of the curves (purple). The four closed circles at 10 or 600 mK verify our measurements as explained in the Fig. 4 caption.

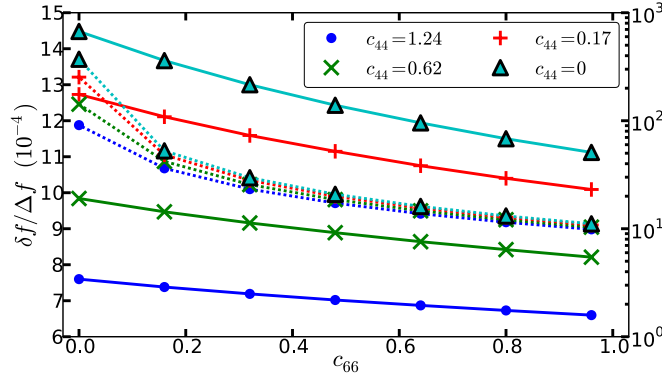


FIG. 7: (color) Change in the TO resonant frequency δf relative to the mass loading Δf as a function of the helium elastic constants c_{44} and $c_{66} = (c_{11} - c_{12})/2$.¹⁹ The calculation is of the same type as in Ref. 5, with a mesh spacing of 0.5 mm. Solid (dashed) lines correspond to the c -axis being perpendicular (parallel) to the rotation axis of the TO and the left (right) vertical axis of the plot. The elastic constants measured at high temperatures at which phonon damping prevents dislocation motion are $c_{44} = 1.24$ and $c_{66} = 0.96$.²⁰ We assume that $\Delta c_{12} = -\Delta c_{11}$, which is one way of satisfying the constraint that the strain energy decreases as the crystal softens.

the hcp structure²² and therefore that c_{44} is the only elastic coefficient that softens in helium crystals. However, the magnitude of the frequency shift we observe in single crystal #2 is too large to be explained by variation of c_{44} alone. According to Ref. 5, the 86% reduction in c_{44} (relative to its intrinsic, low T value) observed in Ref. 11 can produce a frequency shift as large as 0.03% of the mass loading. Single crystal #2 had a three times larger shift of 2 mHz (0.1% of the mass loading). If dislocations can glide parallel to non-basal high density planes, other elastic coefficients could soften, for example $c_{66} = (c_{11} - c_{12})/2$. Calculations of the TO frequency shift as a function of c_{44} and c_{66} are shown in Fig. 7.¹⁹ If the c -axis of the crystal is parallel to the axis of rotation of our TO and c_{44} is close to zero, c_{66} would need to soften by approximately 50% to produce a frequency shift of 0.1% of mass loading, as with single crystal #2. It is also interesting to note that the frequency shift reaches very large values as c_{44} and c_{66} approach zero, for this orientation.

There are some interesting differences between the present results and previous observations. Clark *et al.*¹⁰ observed a frequency shift that was three to five times larger when samples were grown at constant volume (forming polycrystals) than at constant T and P from the superfluid (presumably forming single crystals). This is the opposite of the dependence on crystal quality that we observe, even though the topology the cells in the two experiments is the same and the rigidity of the cells is similar. This difference could be due to the different shapes of the two cells (the interior of our cell has no sharp angles so as to minimize any liquid regions after growth at constant temperature) or the fabrication material (our cell is the only one to be constructed with polished sapphire, producing very smooth walls). We also observe the softening in single crystals at a higher temperature than in other experiments, except perhaps that of Penzev *et al.*²³ We checked that this difference cannot be attributed to a difference in ^3He content. A possible explanation is that the geometry of our cell and our growth process produces crystals with very low dislocation density. As the dislocation density decreases, the average pinning length in the absence of impurities, i.e. the network length L_N , increases. This in turn causes an increase in the pinning temperature $T_p \approx E_B/k_B \ln(a/xL_N)$ (supplement to Ref. 3), where E_B is the ^3He impurity binding energy, a is the atomic spacing along the dislocation, and x is the bulk concentration of ^3He impurities. Thus the onset of the frequency shift should occur at a higher temperature.

Our results therefore suggest that our geometry, cell materials and crystal growth pro-

cedure produce very high quality crystals. It would thus be interesting to directly measure the dislocation density in the crystal. Our results also suggest that elastic coefficients other than c_{44} may change. In view of this, it would also be interesting to measure the temperature dependence of all elastic coefficients of ^4He oriented single crystals, not only the average shear modulus of polycrystals³ or some combination of coefficients in single crystals.^{11,24}

V. ACKNOWLEDGEMENTS

We gratefully acknowledge very helpful conversations with Humphrey Maris and John Beamish. This work is supported by the ERC grant AdG247258-SUPERSOLID and by the NSF grants DMR 0706339 and DMR 1103159.

-
- ¹ E. Kim and M. H. W. Chan, *Nature* **427**, 225 (2004).
 - ² E. Kim and M. H. W. Chan, *Science* **305**, 1941 (2004).
 - ³ J. Day and J. Beamish, *Nature* **450**, 853 (2007).
 - ⁴ S. Balibar, *Nature* **464**, 176 (2010).
 - ⁵ H. J. Maris and S. Balibar, *J. Low Temp. Phys.* **162**, 12 (2011).
 - ⁶ A. C. Clark, J. D. Maynard, and M. H. W. Chan, *Phys. Rev. B* **77**, 184513 (2008).
 - ⁷ J. D. Reppy, *Phys. Rev. Lett.* **104**, 255301 (2010).
 - ⁸ J. T. West, O. Syshchenko, J. Beamish, and M. H. W. Chan, *Nature Phys.* **5**, 598 (2009).
 - ⁹ D. Y. Kim, J. T. West, T. A. Engstrom, N. Mulders, and M. H. W. Chan, *Phys. Rev. B* **85**, 024533 (2012).
 - ¹⁰ A. C. Clark, J. T. West, and M. H. W. Chan, *Phys. Rev. Lett.* **99**, 135302 (2007).
 - ¹¹ X. Rojas, A. Haziot, V. Bapst, S. Balibar, and H. J. Maris, *Phys. Rev. Lett.* **105**, 145302 (2010).
 - ¹² S. Sasaki, F. Caupin, and S. Balibar, *J. Low Temp. Phys.* **153**, 43 (2008).
 - ¹³ S. Balibar, H. Alles, and A. Y. Parshin, *Rev. Mod. Phys.* **77**, 317 (2005).
 - ¹⁴ C. Pantalei, X. Rojas, D. O. Edwards, H. J. Maris, and S. Balibar, *J. Low Temp. Phys.* **159**, 452 (2010).
 - ¹⁵ O. Syshchenko and J. Beamish, *J. Low Temp. Phys.* **150**, 276 (2008).

- ¹⁶ G. W. Morley, A. Casey, C. P. Lusher, B. Cowan, J. Saunders, and J. M. Parpia, *J. Low Temp. Phys.* **126**, 557 (2002).
- ¹⁷ M. J. Graf, Z. Nussinov, and A. V. Balatsky, *J. Low Temp. Phys.* **158**, 550 (2010).
- ¹⁸ E. Kim, Ph.D. thesis, Penn. State University (2004).
- ¹⁹ H. J. Maris (private communication).
- ²⁰ D. S. Greywall, *Phys. Rev. B* **16**, 5127 (1977).
- ²¹ C. Zhou, J.-J. Su, M. J. Graf, C. Reichhardt, A. V. Balatsky, and I. J. Beyerlein (2011), arXiv:1110.0841v1.
- ²² F. Tsuruoka and Y. Hiki, *Phys. Rev. B* **20**, 2702 (1979).
- ²³ A. Penzev, Y. Yasuta, and M. Kubota, *J. Low Temp. Phys.* **148**, 677 (2007).
- ²⁴ Y. Mukharsky, A. Penzev, and E. Varoquaux, *Phys. Rev. B* **80**, 140504 (2009).